

Molecular Dynamics Simulations of Chemically Disordered Ferroelectric (Ba,Sr)TiO₃ with a Semi-Empirical Effective Hamiltonian

Takeshi Nishimatsu¹, Anna Grünebohm², Umesh V. Waghmare³, and Momiji Kubo¹

¹*Institute for Materials Research (IMR), Tohoku University, Sendai 980-8577, Japan*

²*Faculty of Physics and Center for Nanointegration, CENIDE,
University of Duisburg-Essen, 47048 Duisburg, Germany*

³*Theoretical Sciences Unit, Jawaharlal Nehru Centre for Advanced Scientific Research (JNCASR), Bangalore-560064, India*

We present a semi-empirical effective Hamiltonian to capture effects of disorder associated with Ba and Sr cations occupying *A* sites in (Ba_{*x*}Sr_{1-*x*})TiO₃ on its ferroelectric phase transition. Averaging between the parameters of first-principles effective Hamiltonians of end members BaTiO₃ and SrTiO₃, we include a term with an empirical parameter to capture the local polarization and strains arising from the difference between ionic radii of Ba and Sr. Using mixed-space molecular dynamics of the effective Hamiltonian, we determine *T*-dependent ferroelectric phase transitions in (Ba_{*x*}Sr_{1-*x*})TiO₃ which are in good agreement with experiment. Our scheme of determination of semi-empirical parameters in effective Hamiltonian should be applicable to other perovskite-type ferroelectric solid solutions.

I. INTRODUCTION

Barium (Ba) and strontium (Sr) belong to the same column of the periodic table and are chemically very similar. However, ternary perovskites *ABO*₃ based on Ba and Sr at their *A* site can be quite different in their properties: barium titanate (BaTiO₃) is ferroelectric at room temperature, while strontium titanate (SrTiO₃) is paraelectric. It is thought that this is largely because of the difference in their ionic radii¹, $r_{\text{Ba}} = 1.61$ Å and $r_{\text{Sr}} = 1.44$ Å. It can be more understandable through the tolerance factor² defined as

$$t = \frac{r_A + r_O}{\sqrt{2}(r_B + r_O)}, \quad (1)$$

where, r_A , r_B , and r_O are ionic radii of cation $A = \text{Ba}^{2+}$ or Sr^{2+} , cation $B = \text{Ti}^{4+}$, and O^{2-} , respectively. $t = 1.062$ for BaTiO₃ means that the *B*-site Ti ion is too small for its site, the ion can shift off-centering, leading to the occurrence of displacive-type ferroelectricity in the crystal³. t is almost unity ($t = 1.002$) for SrTiO₃, indicating that there is no room for ions to move, ideal cubic perovskite structure become stable at room temperature, and indeed SrTiO₃ does not show ferroelectricity down to the absolute 0 K. Experimentally, at low temperature ($T < 106$ K), SrTiO₃ exhibits very small rotational shift of oxygen octahedra ($\approx 1.6^\circ$) and results in antiferrodistortive *I*₄/*mcm* structure⁴. At very low temperatures, intrinsic quantum paraelectricity⁵ is also found in SrTiO₃.

It has been found experimentally^{6,7} that the three transition temperatures of BaTiO₃, cubic \leftrightarrow tetragonal $T_{\text{C} \leftrightarrow \text{T}}$, tetragonal \leftrightarrow orthorhombic $T_{\text{T} \leftrightarrow \text{O}}$, and orthorhombic \leftrightarrow rhombohedral $T_{\text{O} \leftrightarrow \text{R}}$ decrease almost linearly, when Ba composition x of (Ba_{*x*}Sr_{1-*x*})TiO₃ is reduced from 1. Around pure SrTiO₃ ($x < 0.094$), it is known that the solid solution becomes almost cubic, or more precisely, antiferrodistortive *I*₄/*mcm* structure with very small atomic displacements.

Perovskite-type ferroelectric solid solutions such as (Ba_{*x*}Sr_{1-*x*})TiO₃ are of great interest in the field of dielectrics, since many commercial high-dielectric-constant material structures consist of such solid solutions⁸ and the composition parameter (x here) is adjusted to get desired properties. Therefore, offering a recipe of computational simulations of such solid solutions is important.

In 2006, Walizer *et al.* presented⁹ Monte Carlo simulations with an effective Hamiltonian determined from first-principles calculations of (Ba_{1/2}Sr_{1/2})TiO₃ within a virtual crystal approximation (VCA) and local inhomogeneous strains determined from fully disordered ionic configurations of Ba and Sr of (Ba_{*x*}Sr_{1-*x*})TiO₃. They successfully reproduced the temperature–composition (*T*–*x*) phase diagram, though with a large underestimation of polarization. That underestimation basically came from a local-density approximation (LDA). Moreover, because local inhomogeneous strains around each site were fixed in their analysis and were not allowed to fluctuate thermally, temperature dependence of the effect from ionic configuration was not so clear.

Here, we newly determine a set of parameters for an effective Hamiltonian for (Ba_{*x*}Sr_{1-*x*})TiO₃ from more accurate first-principles calculations, and perform molecular-dynamics (MD) simulations. In our MD simulations, local inhomogeneous strains around each site are not fixed but can fluctuate thermally. We report not only a temperature–composition (*T*–*x*) phase diagram, but also the dependence of polarization and lattice constants on composition.

In Sec. II, we briefly describe the first-principles methods we employ and the formalism and conditions of our MD simulations. In Sec. III, we present results of our MD simulations, and finally summarize our work in Sec. IV.

II. METHODS OF CALCULATION AND FORMALISM

A. First-Principles Methods

Our first-principles calculations are based on the density functional theory (DFT) as implemented in ABINIT code^{10–12}. Bloch wave functions of electrons are expanded in the plane wave basis truncated with a cut-off energy of 60 Hartree, and are sampled on an $8 \times 8 \times 8$ grid of k -points in the first Brillouin zone. We do not use LDA but use “Wu and Cohen”¹³ GGA functional, along with Rappe’s optimized pseudopotentials¹⁴ generated with Opium code¹⁵. A valley-line tracing method¹⁶ is used to determine total energy surface of BaTiO₃ and SrTiO₃. We basically use results of first-principles calculations of BaTiO₃ and SrTiO₃ in Ref. 17.

B. Effective Hamiltonian

We use an effective Hamiltonian, obtained with input from first-principles calculations, for MD simulations. It is essentially the same as that in Refs. 17 and 18,

$$H^{\text{eff}} = \frac{M_{\text{dipole}}^*}{2} \sum_{\mathbf{R}, \alpha} \dot{u}_{\alpha}^2(\mathbf{R}) + \frac{M_{\text{acoustic}}^*}{2} \sum_{\mathbf{R}, \alpha} \dot{w}_{\alpha}^2(\mathbf{R}) + V^{\text{self}}(\{\mathbf{u}\}) + V^{\text{dpl}}(\{\mathbf{u}\}) + V^{\text{short}}(\{\mathbf{u}\}) + V^{\text{elas, homo}}(\eta_1, \dots, \eta_6) + V^{\text{elas, inho}}(\{\mathbf{w}\}) + V^{\text{coup, homo}}(\{\mathbf{u}\}, \eta_1, \dots, \eta_6) + V^{\text{coup, inho}}(\{\mathbf{u}\}, \{\mathbf{w}\}), \quad (2)$$

where the phase space of atomic motion is reduced to a subspace spanned by local soft mode vectors $\mathbf{u}(\mathbf{R})$ and local acoustic displacement vectors $\mathbf{w}(\mathbf{R})$ of each unit cell at \mathbf{R} in a simulation supercell. η_1, \dots, η_6 are the six components of homogeneous strain in Voigt notation ($\eta_1 = e_{xx}$, $\eta_4 = e_{yz}$). $\frac{M_{\text{dipole}}^*}{2} \sum_{\mathbf{R}, \alpha} \dot{u}_{\alpha}^2(\mathbf{R})$ and $\frac{M_{\text{acoustic}}^*}{2} \sum_{\mathbf{R}, \alpha} \dot{w}_{\alpha}^2(\mathbf{R})$ are the kinetic energies of local soft modes and local acoustic displacements along with their effective masses of M_{dipole}^* and M_{acoustic}^* . $V^{\text{self}}(\{\mathbf{u}\})$ is the local-mode self-energy, $V^{\text{dpl}}(\{\mathbf{u}\})$ is the long-range dipole-dipole interaction, $V^{\text{short}}(\{\mathbf{u}\})$ is the short-range harmonic interaction between local soft modes, $V^{\text{elas, homo}}(\eta_1, \dots, \eta_6)$ is the elastic energy from homogeneous strains, $V^{\text{elas, inho}}(\{\mathbf{w}\})$ is the elastic energy from inhomogeneous strains, $V^{\text{coup, homo}}(\{\mathbf{u}\}, \eta_1, \dots, \eta_6)$ is the coupling between the local soft modes and the homogeneous strain, and $V^{\text{coup, inho}}(\{\mathbf{u}\}, \{\mathbf{w}\})$ is the coupling between the soft modes and the inhomogeneous strains. Detailed explanation of symbols in the effective Hamiltonian can be found in Refs. 18, 19, and 20. To decrease the computational time, forces exerted on $\{\mathbf{u}\}$ are calculated in reciprocal space using fast-Fourier transform (FFT) methods^{18,21,22}.

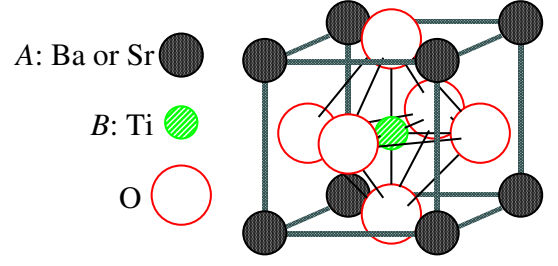


FIG. 1. (Color online) Schematic illustration of perovskite-type crystal structure of (Ba,Sr)TiO₃. $s(\mathbf{R}) = -8, -6, -4, -2, 0, +2, +4, +6, +8$ of Eq. (3) is the number of Ba (+1) or Sr (-1) ions at eight A -sites surrounding a given B -site at \mathbf{R} .

C. Effects of A -site Ordering with Ba or Sr Ions

To include the effects of alloying Ba and Sr with different ionic radii, according to Ref. 9, we count the number of Ba or Sr ions at the 8 A -sites surrounding a given B -site at \mathbf{R} ,

$$s(\mathbf{R}) = \sum_{i=1}^8 \sigma_i \quad (3)$$

as shown in Fig. 1, where $\sigma_i = +1$ or -1 corresponds to the presence of a Ba or Sr ion, respectively. Consequently, value of $s(\mathbf{R})$ ranges $-8, -6, -4, -2, 0, +2, +4, +6, +8$. In contrast to Ref. 9, we introduce a term for *modulation* in local inhomogeneous strains by adding

$$V^{\text{modulation, inho}}(\{\mathbf{w}\}, \{s\}) = c \sum_{\mathbf{R}} \sum_{\alpha=1,2,3} s(\mathbf{R}) \eta_{\alpha}(\mathbf{R}) = \frac{c}{N} \sum_{\mathbf{k}} \sum_{\alpha=x,y,z} \tilde{w}_{\alpha}^*(\mathbf{k}) k_{\alpha} \tilde{s}(\mathbf{k}) \quad (4)$$

to H^{eff} of Eq. (2). Here, c is strength of the *modulation*, N is the number of unit cells in the supercell, \mathbf{k} is wave vector, $\tilde{w}_{\alpha}^*(\mathbf{k})$ is complex conjugate of Fourier transform of $\mathbf{w}(\mathbf{R})$, $\tilde{s}(\mathbf{k})$ is Fourier transform of $s(\mathbf{R})$. To simplify the computation, $V^{\text{modulation, inho}}(\{\mathbf{w}\}, \{s\})$ is calculated in reciprocal space.

Effective hydrostatic pressure of

$$p = b \left(\frac{1}{2} - x \right) \quad (5)$$

is applied to capture the homogeneous strain that alters the lattice constants as a function of x , because the *modulation* of Eq. (4) does not include alternation of the homogeneous strain. Here, b is a constant. Temperature-dependent negative effective pressure $p = -0.005T$ GPa for BaTiO₃, which was applied in Ref. 17 to mimic thermal expansion, is not applied in present work.

In the present MD simulations, only the parameters $V^{\text{modulation, inho}}(\{\mathbf{w}\}, \{s\})$ and p are x -dependent, and other parameters in the effective Hamiltonian of Eq. (2) are kept constant. Such simplification can be successfully employed because Ba and Sr are chemically very similar and different only in their ionic radii. Determination and exact values of the parameters c and b will be discussed in Sec. III B.

D. Molecular-Dynamics (MD) Simulations

MD simulations of $(\text{Ba}_x\text{Sr}_{1-x})\text{TiO}_3$ ($x = 0.0, 0.1, \dots, 0.9, 1.0$) with the effective Hamiltonian are performed with our original MD code **feram**²³. Input files for present simulations are in its free software package of **feram-0.26.01/src/34example-BST/**, and details of the code can be found in Ref. 18. Temperature is kept constant in each temperature step of simulation within a canonical ensemble using the velocity-scaling thermostat for both $\{\mathbf{u}\}$ and $\{\mathbf{w}\}$ with the time step of $\Delta t = 2$ fs. We use a supercell with size of $N = L_x \times L_y \times L_z = 32 \times 32 \times 32$ unit cells and temperature steps of ± 1 K/step in heating-up and cooling-down simulations. In every temperature step, we thermalize the system for 20,000 time steps, after which we use 20,000 time steps to average the properties. The initial configurations of $\{\mathbf{u}\}$ are generated randomly: $\langle u_\alpha \rangle = 0.11\text{\AA}$ ($\alpha = x, y, z$) for heating-up simulations, $\langle u_\alpha \rangle = 0.00\text{\AA}$ for cooling-down simulations, and variance of $\langle u_\alpha^2 \rangle - \langle u_\alpha \rangle^2 = (0.02\text{\AA})^2$ for the both. In the initial configurations, $\{\mathbf{w}\}$ are set to zero. We have checked that the results of these simulations do not depend on initial configurations. A set of $s(\mathbf{R})$ for each x of $(\text{Ba}_x\text{Sr}_{1-x})\text{TiO}_3$ is generated from random configurations of xN Ba and $(x-1)N$ Sr ions.

III. RESULTS AND DISCUSSION

A. Results of First-principles Calculation and Determination of Parameters of H^{eff} of $(\text{Ba}_{1/2}\text{Sr}_{1/2})\text{TiO}_3$

Using the systematic procedure described in Ref. 17, we perform first-principles calculations to determine a set of parameters of H^{eff} for SrTiO_3 (See Table I). We averaged the parameters of H^{eff} of BaTiO_3 in Ref. 17 and those of H^{eff} of SrTiO_3 (See Table I). It is found that this set of parameters indeed reproduces the three transition temperatures of $(\text{Ba}_{1/2}\text{Sr}_{1/2})\text{TiO}_3$ as depicted in Fig. 2(a).

In contrast to the parameters in effective Hamiltonian of Ref. 9 obtained using LDA-based VCA, the present procedure gives improved estimation of equilibrium cubic lattice constant a_0 , and allow simple analysis of the effects of cationic disorder on ferroelectric transitions (See Table I).

TABLE I. Comparison of sets of parameters for BaTiO_3 , SrTiO_3 , and $(\text{Ba}_x\text{Sr}_{1-x})\text{TiO}_3$ (BST). p is the effective pressures applied during MD simulations. Details of these symbols are described in Refs. 18 and 17.

parameter	Ref. 17	present work		Ref. 9
	BaTiO_3	SrTiO_3	BST	VCA
p [GPa]	$-0.005T$	0.0	$6.0(0.5 - x)$	-5.2
a_0 [\AA]	3.986	3.901	3.944	3.901
B_{11} [eV]	126.73	131.33	129.03	129.96
B_{12} [eV]	41.76	36.26	39.01	43.81
B_{44} [eV]	49.24	41.30	45.27	46.94
c [eV]			-0.279	
B_{1xx} [$\text{eV}/\text{\AA}^2$]	-185.35	-102.09	-143.72	-191.72
B_{1yy} [$\text{eV}/\text{\AA}^2$]	-3.2809	0.5299	-1.3755	-3.98
B_{4yz} [$\text{eV}/\text{\AA}^2$]	-14.550	-15.494	-15.022	-5.73
α [$\text{eV}/\text{\AA}^4$]	78.99	22.39	50.69	97.44
γ [$\text{eV}/\text{\AA}^4$]	-115.48	-28.88	-72.18	-143.25
k_1 [$\text{eV}/\text{\AA}^6$]	-267.98	-65.14	-166.56	
k_2 [$\text{eV}/\text{\AA}^6$]	197.50	117.00	157.25	
k_3 [$\text{eV}/\text{\AA}^6$]	830.20	201.68	515.94	
k_4 [$\text{eV}/\text{\AA}^8$]	641.97	139.35	390.66	
M_{dipole}^* [amu]	38.24	43.61	40.93	
M_{acoustic}^* [amu]	46.64	36.70	41.67	
Z^* [e]	10.33	9.28	9.81	9.66
ϵ_∞	6.87	6.46	6.66	5.21
κ_2 [$\text{eV}/\text{\AA}^2$]	8.534	10.316	9.425	6.287
j_1 [$\text{eV}/\text{\AA}^2$]	-2.084	-2.012	-2.048	-2.334
j_2 [$\text{eV}/\text{\AA}^2$]	-1.129	-1.815	-1.472	4.318
j_3 [$\text{eV}/\text{\AA}^2$]	0.689	0.590	0.640	0.817
j_4 [$\text{eV}/\text{\AA}^2$]	-0.611	-0.567	-0.589	-0.461
j_5 [$\text{eV}/\text{\AA}^2$]	0.000	0.000	0.000	0.687
j_6 [$\text{eV}/\text{\AA}^2$]	0.277	0.238	0.258	0.147
j_7 [$\text{eV}/\text{\AA}^2$]	0.000	0.000	0.000	0.073
κ [$\text{eV}/\text{\AA}^2$]	-1.518	-0.126		
$\kappa(\Gamma_{\text{TO}})$ [$\text{eV}/\text{\AA}^2$]	-1.906	-0.254		
$\kappa(X_1)$ [$\text{eV}/\text{\AA}^2$]	17.128	19.215		
$\kappa(X_5)$ [$\text{eV}/\text{\AA}^2$]	-1.422	0.711		
$\kappa(M_{3'})$ [$\text{eV}/\text{\AA}^2$]	-1.143	1.191		
$\kappa(M_{5'})$ [$\text{eV}/\text{\AA}^2$]	16.333	18.424		
$\kappa(R_{25'})$ [$\text{eV}/\text{\AA}^2$]	13.871	16.300		
ξ_z^A	0.166	0.4570		
ξ_z^B	0.770	0.6302		
ξ_z^{OI}	-0.202	-0.3843		
ξ_z^{OII}	-0.202	-0.3843		
ξ_z^{OIII}	-0.546	-0.3139		
Z_{zz}^{*A} [e]	2.741	2.565		
Z_{zz}^{*B} [e]	7.492	7.435		
$Z_{zz}^{*\text{OI}}$ [e]	-2.150	-2.052		
$Z_{zz}^{*\text{OII}}$ [e]	-2.150	-2.052		
$Z_{zz}^{*\text{OIII}}$ [e]	-5.933	-5.892		

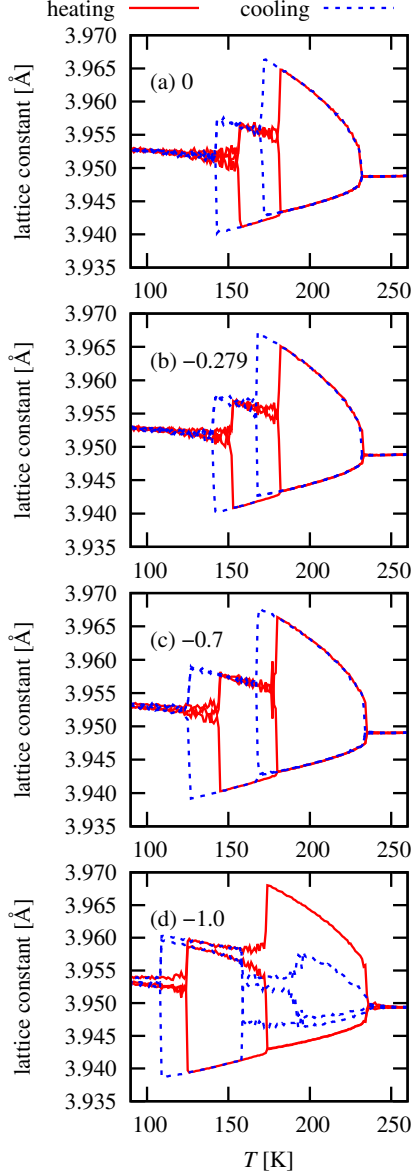


FIG. 2. (Color online) Simulated temperature-dependence of lattice constants of $(\text{Ba}_{1/2}\text{Sr}_{1/2})\text{TiO}_3$ for four different strength of the modulation, $c = 0, -0.279, -0.7, -1.0$, (a)–(d), respectively. The larger $|c|$, the lower $T_{\text{O} \leftrightarrow \text{R}}$.

B. Determination of Parameters for $(\text{Ba}_x\text{Sr}_{1-x})\text{TiO}_3$ Alloy

To simulate an alloy or solid solution $(\text{Ba}_x\text{Sr}_{1-x})\text{TiO}_3$, we determine the modulation strength c in Eq. (4) as

$$c = -\frac{1}{16} \frac{a_{\text{BTO}} - a_{\text{STO}}}{a_{\text{BST}}} (B_{11} + 2B_{12}) = -0.279 \text{ [eV]}. \quad (6)$$

When $s(\mathbf{R}) = \pm 8$, local inhomogeneous strains of

$$\eta_1 = \eta_2 = \eta_3 = \pm \frac{1}{2} \frac{a_{\text{BTO}} - a_{\text{STO}}}{a_{\text{BST}}} \quad (7)$$

minimize the energy:

$$E(\{\eta_\alpha\}_{\text{local}}) = \frac{1}{2} B_{11} (\eta_1^2 + \eta_2^2 + \eta_3^2) + B_{12} (\eta_2 \eta_3 + \eta_3 \eta_1 + \eta_1 \eta_2) + \frac{1}{2} B_{44} (\eta_4^2 + \eta_5^2 + \eta_6^2) + cs(\eta_1 + \eta_2 + \eta_3). \quad (8)$$

Here, $a_{\text{BTO}} = 3.986 \text{ \AA}$ is the calculated cubic lattice constant of BaTiO_3 , $a_{\text{STO}} = 3.901 \text{ \AA}$ is that of SrTiO_3 , and $a_{\text{BST}} = (a_{\text{BTO}} + a_{\text{STO}})/2 = 3.944 \text{ \AA}$, and B_{11} , B_{12} , and B_{44} are the elastic constants of $(\text{Ba}_{1/2}\text{Sr}_{1/2})\text{TiO}_3$ expressed in energy unit ($B_{11} = a_{\text{BST}}^3 C_{11}$, $B_{12} = a_{\text{BST}}^3 C_{12}$, and $B_{44} = a_{\text{BST}}^3 C_{44}$). In Fig. 2, results of heating-up and cooling-down MD simulations with four different values of $c = 0, -0.279, -0.7$, and -1.0 [eV] are given for $x = 1/2$, i.e. $(\text{Ba}_{1/2}\text{Sr}_{1/2})\text{TiO}_3$ for which the largest influence of disordered ionic configurations has to be expected. We find lower transition temperature between orthorhombic and rhombohedral structures, i.e. $T_{\text{O} \leftrightarrow \text{R}}$, for larger $|c|$. The other two transition temperatures $T_{\text{C} \leftrightarrow \text{T}}$ and $T_{\text{T} \leftrightarrow \text{O}}$ remain almost unchanged. This may be because $T_{\text{O} \leftrightarrow \text{R}}$ is the lowest transition temperature among the three, and local inhomogeneous strains around each site are almost frozen into the lowest energy structure. However, the difference in $T_{\text{O} \leftrightarrow \text{R}}$ between $c = 0$ and $c = -0.279 \text{ eV}$ is only 3 K. In Fig. 2(d), we find strange behavior in tetragonal phase for $c = -1.0$ which may be unrealistically negatively large.

We first set the constant b in the effective pressure of Eq. (5) so that average lattice constant becomes the same as BaTiO_3 for $x = 1.0$ and SrTiO_3 for $x = 0.0$ as

$$b = \frac{a_{\text{BTO}} - a_{\text{STO}}}{a_{\text{BST}}} 3K = 11.65 \text{ [GPa]}, \quad (9)$$

where $K = (B_{11} + 2B_{12})/(3a_{\text{BST}}^3)$ is bulk modulus. However, $b = 11.65 \text{ [GPa]}$ gives too high transition temperatures for $x = 1$, i.e. BaTiO_3 . Therefore, we determine this b empirically, as $b = 6.0 \text{ [GPa]}$. The reason for this may be the overestimation of the coupling between homogeneous strain and polarization.

C. Results of Molecular-Dynamics Simulations

Using the set of parameters determined above, we perform heating-up and cooling-down MD simulations. In Fig. 3, a calculated temperature–composition (T – x) phase diagram is presented. Heating-up and cooling-down transition temperatures are averaged when corresponding transition has temperature hysteresis between the heating-up and cooling-down simulations.

For $x > 0.25$, the almost linear x -dependence of all three transition temperatures is well reproduced by our approach. For x below 0.25 the experimentally observed transition temperatures decrease with a larger slope and the alloy is no longer ferroelectric⁷ for $x < 0.094$. In this concentration range of $x < 0.25$, the antiferrodistortive

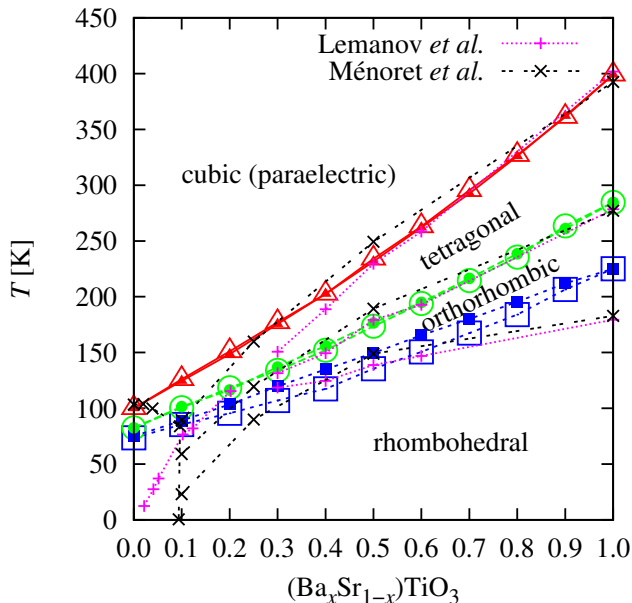


FIG. 3. (Color online) Simulated temperature-composition (T - x) phase diagram. Heating-up and cooling-down transition temperatures are averaged when the corresponding transition has a hysteresis. Empty marks are from simulations with *modulation* of $c = -0.7$ eV. Filled marks are from simulations without *modulation* $c = 0$. Note that results of $c = -0.7$ eV are shown here, because the difference between $c = 0$ and $c = -0.279$ eV cannot be clearly seen in this scale. Two experimental results by Lemanov *et al.*⁶ and Mñoret *et al.*⁷ are also plotted for comparison.

instability found in pure SrTiO_3 may play an important role and the instability reduces transition temperatures non-linearly, and finally for pure SrTiO_3 the system is a quantum paraelectric. Both effects are not accessible in our classical MD simulations neglecting rotations of octahedra.

Simulated x -dependence of lattice constants a and c at room temperature (300 K) is compared with experimental values⁸ in Fig. 5. Though the absolute values have good agreement, more moderate x -dependence of lattice constants of our simulations than the experiment is coming from the empirical correction to b from 11.65 to 6.0 GPa used here. Overestimation of c/a of this MD simulation is coming from the error in first-principles calculations and unavoidable within current techniques of DFT theories²⁴.

Simulated x -dependence of polarization $|P|$ is also compared with the experimentally observed values⁷ in Fig. 5. It is seen that our simulation slightly overestimates $|P|$ for the whole range of x and for any phases, but trends for $x > 0.094$ are quite reasonable. The main reason for this may come from the unavoidable overestimation of c/a and resulting overestimation of $|P|$ in first-principles calculations. Moreover, as shown in Fig. 6, *true* dipole moment per unit cell $P(u)$ deviates from lin-

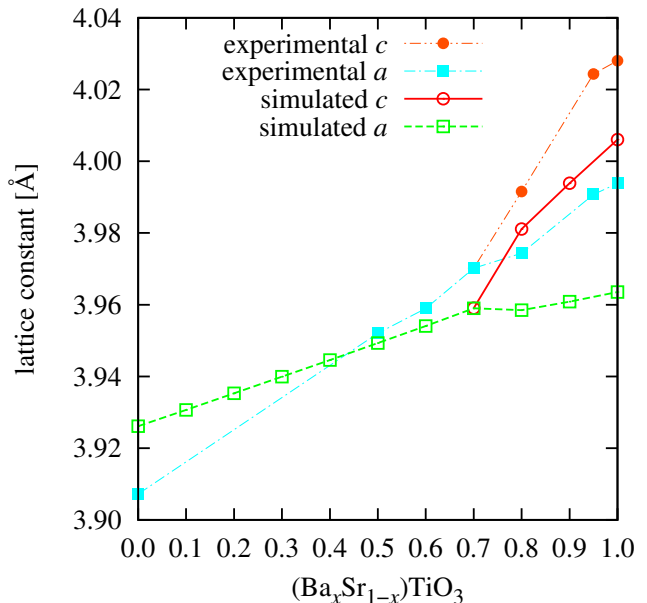


FIG. 4. (Color online) Simulated x -dependence of lattice constants a (open square marks) and c (open circle marks) at room temperature (300 K). For comparison, experimentally observed values by McQuarrie⁸ are also plotted (filled marks).

earity at large u both in BaTiO_3 and SrTiO_3 , and it may also explain the overestimation of $|P|$ in Fig. 5. In Fig. 6, *true* dipole moment as a function of u for atomic displacements along $[001]$ distortion calculated with the Berry-phase theory²⁵ is compared with Z^*u in H^{eff} of Eq. (2).

IV. SUMMARY

In this work, we presented a new set of parameters of an effective Hamiltonian for $(\text{Ba}_x\text{Sr}_{1-x})\text{TiO}_3$ solid-solution with input largely from the results of first-principles calculations, including the *modulation* in local inhomogeneous strains due to Ba:Sr disorder. Using heating-up and cooling-down MD simulations we have obtained $x - T$ phased diagram. Though two parameters have been determined semi-empirically, results of our simulations and experimentally observed values are in good agreement for the dependence of transition temperatures, lattice constants a and c , and polarization on composition x . It is found that x -dependent properties of $(\text{Ba}_x\text{Sr}_{1-x})\text{TiO}_3$ are determined mainly through the change in homogeneous lattice constants and that influence of *modulation* on local inhomogeneous strains is relatively weak.

Our procedure of first-principles calculations, determination of parameters, and MD calculations should be applicable to other perovskite-type ferroelectric solid solutions such as $(\text{K},\text{Na})\text{NbO}_3$, $(\text{Ba},\text{Sr},\text{Ca})\text{TiO}_3$, etc.

ACKNOWLEDGMENTS

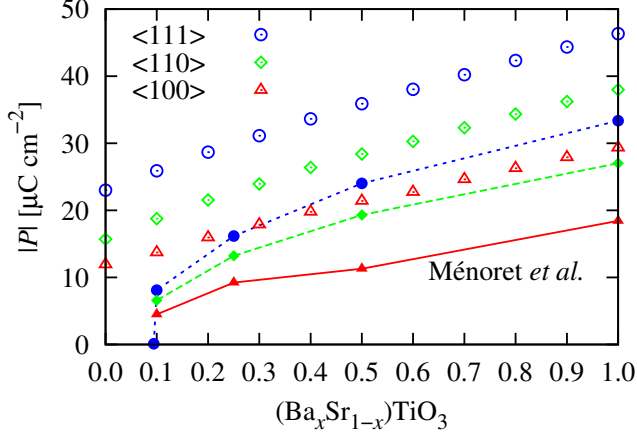


FIG. 5. (Color online) Simulated composition ratio x -dependence of polarization $|P|$ (open marks). $|P|$ is measured at the middle of the two transition temperatures, $(T_{C \leftrightarrow T} + T_{T \leftrightarrow O})/2$ for $|P_{\langle 100 \rangle}|$ of the tetragonal phase or $(T_{T \leftrightarrow O} + T_{O \leftrightarrow R})/2$ for $|P_{\langle 110 \rangle}|$ of the orthorhombic phase, or half of $T_{O \leftrightarrow R}$ for $|P_{\langle 111 \rangle}|$ of the rhombohedral phase. For comparison, experimentally observed values by Ménéret *et al.*⁷ are also plotted (filled marks connected with lines).

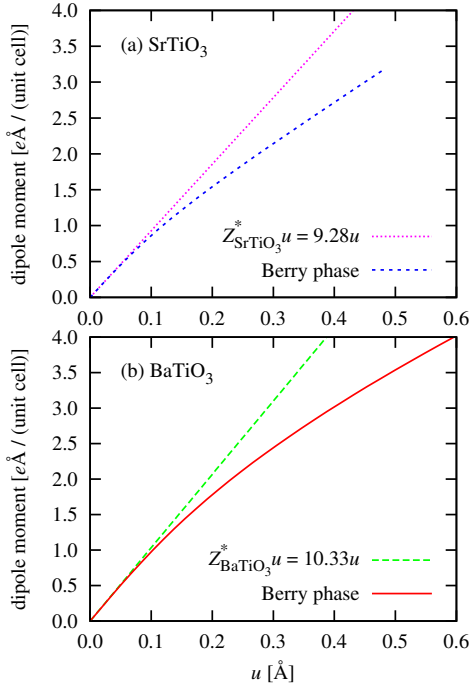


FIG. 6. (Color online) Using the Berry-phase theory²⁵, dipole moments per unit cell as a function of u for atomic displacements along $[001]$ distortion are calculated for (a) SrTiO_3 and (b) BaTiO_3 . Z^*u in H^{eff} of Eq. (2) are also plotted for comparison. 1.0 eÅ in a unit cell of volume $(4.0 \text{ Å})^3$ corresponds to $25 \text{ μC} \cdot \text{cm}^{-2}$.

Computational resources were provided by the Center for Computational Materials Science, Institute for Materials Research (CCMS-IMR), Tohoku University. We thank the staff at CCMS-IMR for their constant effort. This study is financially supported by the German Research Foundation, DFG SPP 1599. This study was also supported in part by MEXT as a social and scientific priority issue (Creation of new functional devices and high-performance materials to support next-generation industries) to be tackled by using post-K computer. U.V.W. acknowledges support from a JC Bose National Fellowship of the Department of Science and Technology, Government of India. We acknowledge collaboration and useful discussion with Anil Kumar.

¹ R. D. Shannon, Acta Cryst. A **32**, 751 (1976).

² V. M. Goldschmidt, Akad. Oslo Math-Natur. **2**, 7 (1926).

- ³ D. Fu and M. Itoh, *Ferroelectrics – Material Aspects* (IN-TECH, Rijeka, 2011) chapter 20.
- ⁴ H. Fujishita, Y. Shiozaki, and E. Sawaguchi, *J. Phys. Soc. Jpn.* **46**, 581 (1979).
- ⁵ K. A. Müller and H. Burkard, *Phys. Rev. B* **19**, 3593 (1979).
- ⁶ V. V. Lemanov, E. P. Smirnova, P. P. Syrnikov, and E. A. Tarakanov, *Phys. Rev. B* **54**, 3151 (1996).
- ⁷ C. Ménoret, J. M. Kiat, B. Dkhil, M. Dunlop, H. Dammak, and O. Hernandez, *Phys. Rev. B* **65**, 224104 (2002).
- ⁸ M. McQuarrie, *J. Am. Ceram. Soc.* **38**, 444 (1955).
- ⁹ L. Walizer, S. Lisenkov, and L. Bellaiche, *Phys. Rev. B* **73**, 144105 (2006).
- ¹⁰ X. Gonze, J.-M. Beuken, R. Caracas, F. Detraux, M. Fuchs, G.-M. Rignanese, L. Sindic, M. Verstraete, G. Zerah, F. Jollet, M. Torrent, A. Roy, M. Mikami, P. Ghosez, J.-Y. Raty, and D. C. Allan, *Comput. Mater. Sci.* **25**, 478 (2002).
- ¹¹ X. Gonze, B. Amadon, P.-M. Anglade, J.-M. Beuken, F. Bottin, P. Boulanger, F. Bruneval, D. Caliste, R. Caracas, M. Cote, T. Deutsch, L. Genovese, P. Ghosez, M. Giantomassi, S. Goedecker, D. R. Hamann, P. Hermet, F. Jollet, G. Jomard, S. Leroux, M. Mancini, S. Mazevet, M. J. T. Oliveira, G. Onida, Y. Pouillon, T. Rangel, G.-M. Rignanese, D. Sangalli, R. Shaltaf, M. Torrent, M. J. Verstraete, G. Zerah, and J. W. Zwanziger, *Comput. Phys. Commun.* **180**, 2582 (2009).
- ¹² X. Gonze, F. Jollet, F. Abreu Araujo, D. Adams, B. Amadon, T. Applencourt, C. Audouze, J.-M. Beuken, J. Bieder, A. Bokhanchuk, E. Bousquet, F. Bruneval, D. Caliste, M. Côté, F. Dahm, F. Da Pieve, M. Delaveau, M. Di Gennaro, B. Dorado, C. Espejo, G. Geneste, L. Genovese, A. Gerossier, M. Giantomassi, Y. Gillet, D. R. Hamann, L. He, G. Jomard, J. Laflamme Janssen, S. Le Roux, A. Levitt, A. Lherbier, F. Liu, I. Lukačević, A. Martin, C. Martins, M. J. T. Oliveira, S. Poncé, Y. Pouillon, T. Rangel, G.-M. Rignanese, A. H. Romero, B. Rousseau, O. Rubel, A. A. Shukri, M. Stankovski, M. Torrent, M. J. Van Setten, B. Van Troeye, M. J. Verstraete, D. Waroquiers, J. Wiktor, B. Xu, A. Zhou, and J. W. Zwanziger, *Comput. Phys. Commun.* **205**, 106 (2016).
- ¹³ Z. G. Wu and R. E. Cohen, *Phys. Rev. B* **73**, 235116 (2006).
- ¹⁴ A. M. Rappe, K. M. Rabe, E. Kaxiras, and J. D. Joannopoulos, *Phys. Rev. B* **41**, 1227 (1990).
- ¹⁵ *Opium - pseudopotential generation project*, <http://opium.sourceforge.net/> (1998–2014).
- ¹⁶ T. Hashimoto, T. Nishimatsu, H. Mizuseki, Y. Kawazoe, A. Sasaki, and Y. Ikeda, *Jpn. J. Appl. Phys.* **43**, 6785 (2004).
- ¹⁷ T. Nishimatsu, M. Iwamoto, Y. Kawazoe, and U. V. Waghmare, *Phys. Rev. B* **82**, 134106 (2010).
- ¹⁸ T. Nishimatsu, U. V. Waghmare, Y. Kawazoe, and D. Vanderbilt, *Phys. Rev. B* **78**, 104104 (2008).
- ¹⁹ R. D. King-Smith and D. Vanderbilt, *Phys. Rev. B* **49**, 5828 (1994).
- ²⁰ W. Zhong, D. Vanderbilt, and K. M. Rabe, *Phys. Rev. B* **52**, 6301 (1995).
- ²¹ U. V. Waghmare, E. J. Cockayne, and B. P. Burton, *Ferroelectrics* **291**, 187 (2003).
- ²² U. V. Waghmare, *Acc. Chem. Res.* **47**, 3242 (2014).
- ²³ T. Nishimatsu, *feram at SourceForge.net*, <http://loto.sourceforge.net/feram/> (2007–2016).
- ²⁴ J. Sun, R. C. Remsing, Y. Zhang, Z. Sun, A. Ruzsinszky, H. Peng, Z. Yang, A. Paul, U. Waghmare, X. Wu, M. L. Klein, and J. P. Perdew, *Nat. Chem.*, 2535 (2016).
- ²⁵ R. D. King-Smith and D. Vanderbilt, *Phys. Rev. B* **47**, 1651 (1993).